Supporting Information for "Geophysical investigations of habitability in ice-covered ocean worlds"

Contents of this file

1. Text S1 to S7

2. Figures S1 to S8

Introduction This supplement explains the technical details of the model elements. Most of the model components described below have been developed in greater detail in prior publications. Supplemental figures provide further detail of the assumed mineral thermodynamic properties (Figs. S1-S3) and associated planetary properties (Figs. S4-S8).

Corresponding author: S. D. Vance MS 321-540, 4800 Oak Grove Drive, Jet Propulsion Laboratory, Pasadena, CA 91109, USA. (svance@jpl.nasa.gov)

Text S1: Bulk Sound Speed in Ice

[*Choukroun and Grasset*, 2010] fit the specific volumes for the phases of water as

$$V_{sp}(P,T) = V_0\zeta_1(T)\zeta_2(P), \tag{1}$$

with

$$\zeta_1 = 1 + a_0 \tanh(a_1(T - T_{ref})) \tag{2}$$

$$\zeta_2 = b_0 + b_1(1 - \tanh(b_2 P)) \tag{3}$$

in which the a's and b's, T_{ref}, and V_0 are fitting parameters. The pressure derivative is

$$\frac{\partial V_{sp}}{\partial P} = V_0\zeta_1(T)\frac{d\zeta_2(P)}{dP} \tag{4}$$

$$\frac{d\zeta_2}{dP} = -b_1 b_2 \operatorname{sech}^2(b_2 P) \tag{5}$$

The corresponding pressure derivative of density is

$$\left(\frac{\partial \rho}{\partial P}\right)_T = -\frac{1}{V_{sp}^2}\frac{\partial V_{sp}}{\partial P} \tag{6}$$

Text S2: Mass and Gravitational Moment of Inertia

The bulk mass of the planet M is the sum of nested spherical shells of radius r (thickness dr) with constant density $\rho(r)$:

$$\begin{aligned} M = \int_M dm &= 4\pi \int_{R_{sil}}^{R} \rho(r) r^2 dr + \frac{4\pi}{3}\rho_{sil} R_{sil}^3 \\ &= M_{H_2O} + \frac{4\pi}{3}\rho_{sil} R_{sil}^3 \end{aligned} \tag{7}$$

where the M_{H_2O} includes the mass of the low-pressure ice upper layer, the ocean, and the high-pressure ice layers. The moment of inertia is:

$$C = \int_M x^2 dm = \iiint r^4 \rho(r,\theta,\psi) sin^3(\theta) dr d\theta d\psi \quad (8)$$
$$= \frac{8\pi}{3} \int_{R_{sil}}^{R} \rho(r) r^4 dr + \frac{8\pi}{15} \rho_{sil} R_{sil}^5$$
$$= C_{H_2O} + \frac{8\pi}{15} \rho_{sil} R_{sil}^5$$

where x is the distance of the element of mass (dm) from the spin axis. Starting from the surface ($R_{sil} = R - dr$), the radius of the silicate interface is decreased by dr. The overlying mass (M_{H_2O}) and moment of inertia (C_{H_2O}) are recomputed with each step. The solution of the interface radius (R_{sil}) provides the silicate density (ρ_{sil}) from Eq. 7. We use this value to calculate the moment of inertia from Eq. 8 for specified values of the temperature at the base of the ice I layer (T_b) and specified values of fluid salinity.

Text S3: Silicate Interior and Metallic Core

To predict the radii of the silicate/H_2O interface (R_{sil}) and iron core (R_{iron}), the model prescribes the densities of the silicates (ρ_{sil}) and the iron core (ρ_{core}). The moment of inertia is then computed from:

$$M_{iron} = M - M_{H_2O} - \frac{4\pi}{3} \rho_{sil} \left(R_{sil}^3 - R_{iron}^3 \right) \quad (9)$$
$$R_{iron} = \left(\frac{M - M_{H_2O} - \frac{4\pi}{3} \rho_{sil} R_{sil}^3}{\frac{4\pi}{3} (\rho_{iron} - \rho_{sil})} \right)^{1/3} \quad (10)$$
$$C = C_{H_2O} + \frac{8\pi}{15} \left(\rho_{sil} (R_{sil}^5 - R_{iron}^5) + \rho_{iron} R_{iron}^5 \right) \quad (11)$$

If no iron core is present (as stipulated by the model), R_{sil} is a function of ρ_{sil} and C. In all cases, the model finds the range of values allowed by the bounded moment of inertia and chooses those corresponding to the nominal value of C.

Text S3: Thermal Conduction in Ices

Thermally conductive profiles in ice Ih assume temperature-dependent conductivity of the form $k = D/T$, with temperature represented as a function of depth z as

$$T(z) = {T_b}^{\frac{z}{z_b}} {T_o}^{1-\frac{z}{z_b}}, \tag{12}$$

and corresponding heat flux at the ice I-water interface (z_b and T_b),

$$q_b = D\frac{\ln T_b/T_s}{z_b}. \tag{13}$$

Assuming D =632 W m^{-1} for ice Ih provides accuracy of better than 10% in the range of temperatures from 100-270 K. Scalings other than T^{-1} from *Andersson and Inaba* [2005] are refit to match the middle of the provided range of temperature with a loss of accuracy of less than 5%. For the calculation of solid state convection (S5), k is computed from the fits recommended by *Andersson and Inaba* [2005].

Text S4: Thermal Conduction in Rock

The temperature profile in the rocky interior is computed by the same method as in *Cammarano et al.* [2006]:

$$T(r) = T_0 + \frac{\rho_{rock} H}{6k}(a^2 - r^2) + \left(\frac{\rho_{rock} H r_b^3}{3k} - \frac{q_b r_b^2}{k}\right)\left(\frac{1}{a} - \frac{1}{r}\right) \tag{14}$$

The relevant inputs to PlanetProfile are: ρ_{rock}, the mean silicate density specified as an input: H, the rate of heat production per unit mass ($H = Q/M$, determined from input of Q in W m^{-2}); and k, the thermal conductivity of the rock. The remaining variables are determined by the model: T_0, the temperature at the top of the silicate layer; and a and r_b, the radius at the top and bottom of the silicate layer, respectively. The heat flow at the base of the rock layer (q_b) is set to zero. Thermal conductivity is the same as that specified by *Cammarano et al.* [2006]: $k = 4.0$ W (m K)$^{-1}$.

Text S5: Solid State Convection in Ices

Solid state convection in ice Ih is from the parameterization of *Deschamps and Sotin* [2001], based on numerical experiments and known material properties. The critical Rayleigh number

$$Ra = \frac{\alpha \rho g \Delta T h^3}{\kappa \mu} \tag{15}$$

is determined at the characteristic temperature of the well-mixed convective interior of the ice:

$$T_c = B\left[\sqrt{1 + \frac{2}{B}(T_m - C)} - 1\right], B = \frac{E}{2Rc_1}, C = c_2 \Delta T \tag{16}$$

in which T_m is the characteristic melting temperature, specified as temperature at the ice-liquid interface, E is the activation energy of the material (Table 1), R is the ideal gas constant (8.314 J mole^{-1} K^{-1}), $c_1 = 1.43$, $c_2 = -0.03$, and $\Delta T = T_m - T_{top}$. The Newtonian viscosity is

$$\mu = \mu_0 \exp\left[A\left(\frac{T_m}{T} - 1\right)\right], A = \frac{E}{RT_m} \tag{17}$$

with coefficient μ_0 specified in Table 1.

The lower thermal boundary layer scales with Rayleigh number as $Ra_\delta = 0.28 Ra^{0.21}$. The boundary layer's thickness is

$$\delta = \left[\frac{\mu_c \kappa}{\alpha \rho g (T_m - T_c)} Ra_\delta\right]^{1/3} \tag{18}$$

and the corresponding heat flux is

$$Q = \frac{k(T_m - T_c)}{\delta}. \tag{19}$$

The temperature of the overlying brittle lithosphere is scaled as $T_{lith} = T_{top} + 0.3\Delta T$ The thermal boundary layer thickness is

$$e_{TBL} = \frac{k_{ice}(T_{lith} - T_{top})}{Q}. \tag{20}$$

Text S6: Computation of tidal deformation The viscoelastic deformation of icy moons under the action of periodic tidal forces is computed following the method of *Tobie et al.* [2005], using the elastic formulation of *Takeuchi et al.* [1972] transposed to the viscoelastic case. The internal solid layers are assumed to be viscoelastic and compressible. The internal ocean is assumed to be inviscid and non-dissipative. The density profile and elastic properties in each layer are computed using PlanetProfile. For the viscosity profile in the ice layers, we used the rheological law B.11 and the rheological parameters provided in Table S1. For the rocky core, we assume a constant viscosity equal to 10^{22} Pa.s. From these profiles, the Poisson equation and the equations of motion are solved for small perturbations in the frequency domain, assuming a compressible Andrade rheology [*Castillo-Rogez et al.*, 2011]. The complex compliance, which defines the complex shear modulus, is given for an Andrade model by:

$$J(\chi) = \frac{1}{\chi} - \frac{i}{\eta\chi} + \beta\,(i\chi)^{-\alpha}\,\Gamma\,(1+\alpha)\,, \tag{21}$$

where μ is the shear modulus ($\mu = \rho V_s^2$), η is the viscosity, χ is the tidal frequency ($\chi = 2(\omega - n)$), ω and n being the spin rate and mean orbital motion respectively, α and β are parameters describing the frequency dependence and the amplitude of the transient response, respectively. Comparisons with available experimental data for ice and rock [*Castillo-Rogez et al.*, 2011], and with applications to the Earth [*Dumoulin et al.*, 2017], indicate that the Andrade model is a good approximation to describe the anelastic attenuation at tidal frequencies. For the α parameter, we explore a range of values varying between 0.2 and 0.3, which frames the typical value required to explain the Q factor of the Earth's mantle [*Dumoulin et al.*, 2017]. We assume that $\beta \simeq \mu^{\alpha-1}\eta^{-\alpha}$, following the approximation of *Castillo-Rogez et al.* [2011].

The Love numbers (k_2 and h_2) characterizing the potential perturbation and surface displacement, respectively, and the dissipation function (Q^{-1}) are computed by integrating the radial functions associated with the radial and tangential displacements (y_1 and y_3, respectively), the radial and tangential stresses (y_2 and y_4), the gravitational potential (y_5), and the continuity of the gravitational potential, (y_6), as defined by *Takeuchi et al.* [1972]. The deformation of the liquid water ocean is assumed to be static; the simplified formulation of *Saito* [1974], relying on only two radial functions (y_5 and y_7) is thus employed. The solution in the solid part of the interior is expressed as the linear combination of three independent solutions, which reduces to two independent solutions in the fluid part. The system of six differential equations is solved by integrating the three independent solutions using a fifth order Runge-Kutta method, with adjustive step size control, from the center ($r = 0$ km) to the satellite surface ($r = R_S$), and by applying the appropriate boundary conditions (see for more details: *Takeuchi et al.* [1972]; *Saito* [1974]; *Tobie et al.* [2005]). The complex Love numbers (k_2 and h_2) are determined from the radial functions, $y_5(R_S)$ and $y_1(R_S)$ respectively, at the satellite surface ($r = R_S$), and the global dissipation function (Q^{-1}) by the ratio between the imaginary part and the modulus of k_2:

$$k_2 = y_5(R_S) - 1;\ h_2 = y_1(R_S)g(R_S);\ Q^{-1} = \Im(k_2)/\|k_2\|. \tag{22}$$

References

Andersson, O., and A. Inaba (2005), Thermal conductivity of crystalline and amorphous ices and its implications on amorphization and glassy water, *Physical Chemistry Chemical Physics*, *7*(7), 1441, doi:10.1039/b500373c.

Cammarano, F., V. Lekic, M. Manga, M. Panning, and B. Romanowicz (2006), Long-period seismology on europa: 1. physically consistent interior models, *Journal of Geophysical Research: Planets*, *111*(E12), n/a–n/a, doi:10.1029/2006je002710.

Castillo-Rogez, J. C., M. Efroimsky, and V. Lainey (2011), The tidal history of Iapetus: Spin dynamics in the light of a refined dissipation model, *Journal of Geophysical Research*, *116*(E9), doi:10.1029/2010je003664.

Choukroun, M., and O. Grasset (2010), Thermodynamic data and modeling of the water and ammonia-water phase diagrams up to 2.2 GPa for planetary geophysics, *The Journal of Chemical Physics*, *133*(14), 144,502, doi:10.1063/1.3487520.

Deschamps, F., and C. Sotin (2001), Thermal convection in the outer shell of large icy satellites, *Journal of Geophysical Research: Planets*, *106*(E3), 5107–5121, doi:10.1029/2000je001253.

Dumoulin, C., G. Tobie, O. Verhoeven, P. Rosenblatt, and N. Rambaux (2017), Tidal constraints on the interior of Venus, *Journal of Geophysical Research: Planets*, *122*(6), 1338–1352, doi:10.1002/2016je005249.

Durham, W. B., S. H. Kirby, and L. A. Stern (1997), Creep of water ices at planetary conditions: A compilation, *Journal of Geophysical Research: Planets*, *102*(E7), 16,293–16,302, doi:10.1029/97je00916.

Gagnon, R. E., H. Kiefte, M. J. Clouter, and E. Whalley (1990), Acoustic velocities and densities of polycrystalline ice Ih, II, III, V, and VI by Brillouin spectroscopy, *The Journal of Chemical Physics*, *92*(3), 1909–1914, doi:10.1063/1.458021.

Saito, M. (1974), Some problems of static deformation of the earth., *Journal of Physics of the Earth*, *22*(1), 123–140, doi:10.4294/jpe1952.22.123.

Takeuchi, H., M. Saito, and B. Bolt (1972), Seismic surface waves, *Methods in computational physics*, *11*, 217–295.

Tobie, G., A. Mocquet, and C. Sotin (2005), Tidal dissipation within large icy satellites: Applications to Europa and Titan, *Icarus*, *177*(2), 534–549, doi: 10.1016/j.icarus.2005.04.006.

Table 1. Ice Material Parameters

Crystalline Phase	D^b W m^{-1}	μ_0^b Pa s	E^c kJ mol^{-1}	K_S^d GPa	μ^d GPa
I	632	5×10^{13}	60	9.96	3.6
II	418	1×10^{18}	77	13.89	6.2
III	242	5×10^{12}	127	9.87	4.6
V	328	5×10^{14}	136	14.19	6.1
VI	183	5×10^{14}	110	18.14	7.5

[a]adapted from *Andersson and Inaba* [2005] Table 1; [b]*Durham et al.* [1997] Fig. 4b;

[c]*Deschamps and Sotin* [2001]; [d]*Gagnon et al.* [1990]

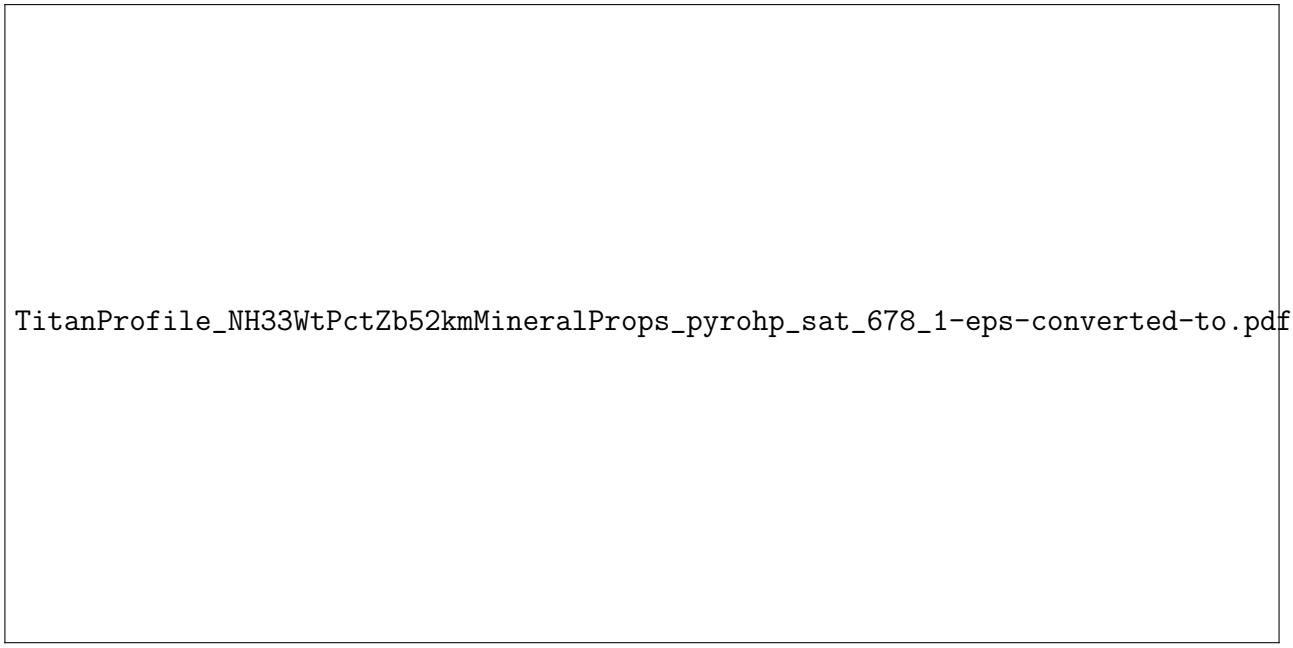

Figure S1. The saturated pyrolite composition containing Na_2O

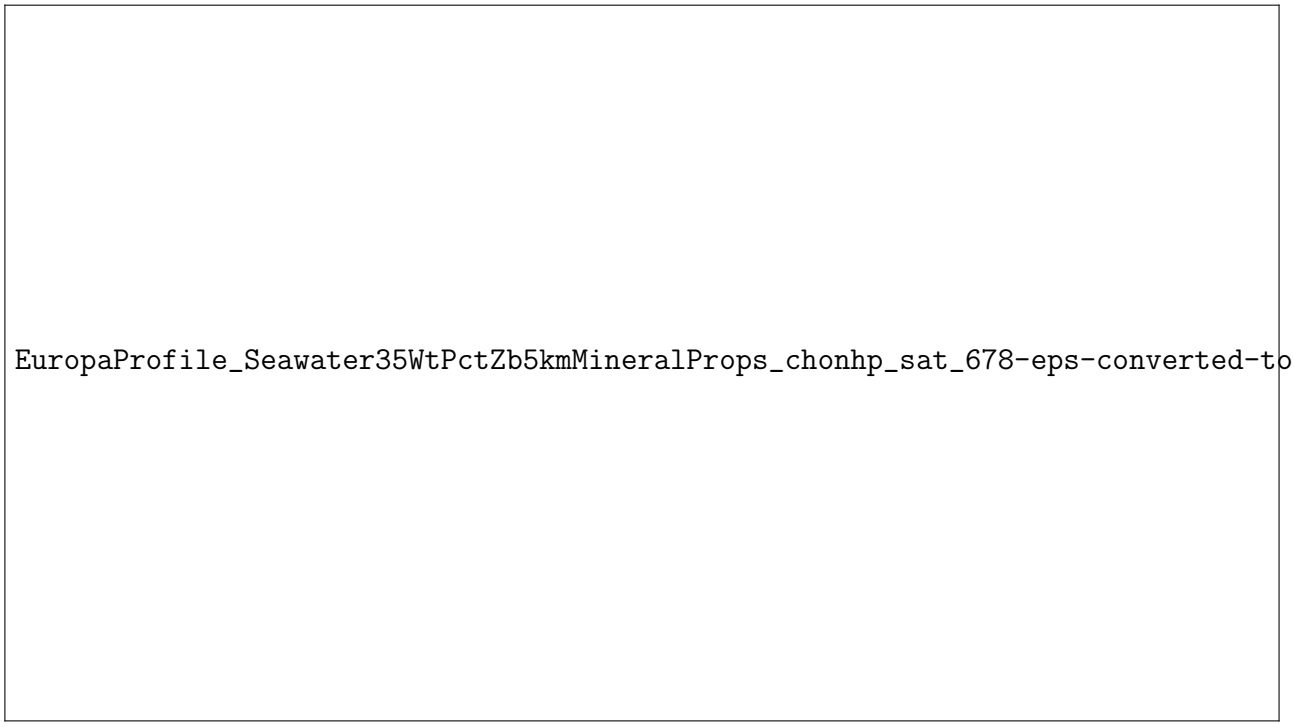

Figure S2. The saturated chondrite composition containing Na_2O

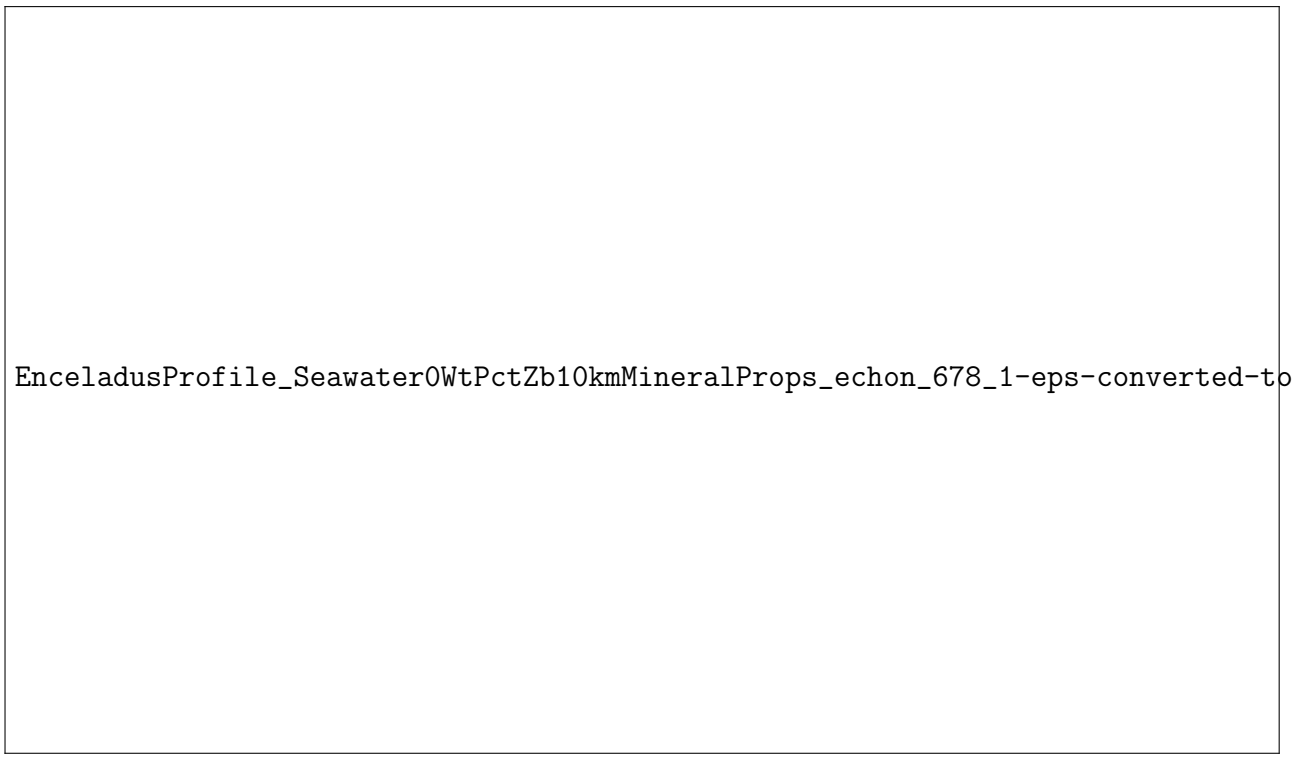

Figure S3. The anhydrous chondrite composition

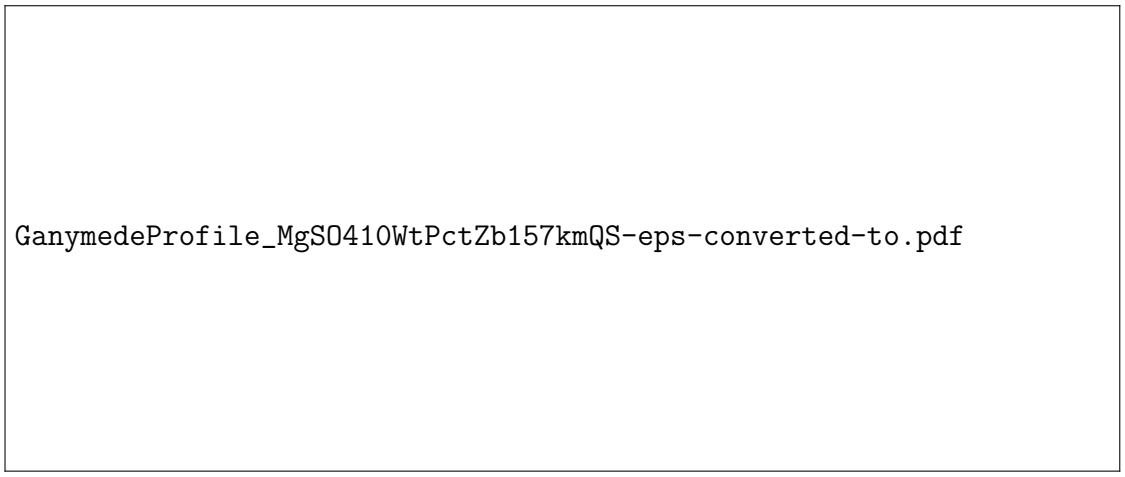

Figure S4. Ganymede: global interior structure for an ocean with 10 wt% $MgSO_4$(aq) and ice Ih thickness of 157 km. Left: V_S (lines) and V_P (dashes). Middle: Pressure (lines), temperature (dashes) and density (dot-dashes). Right: Anelasticity.

lines

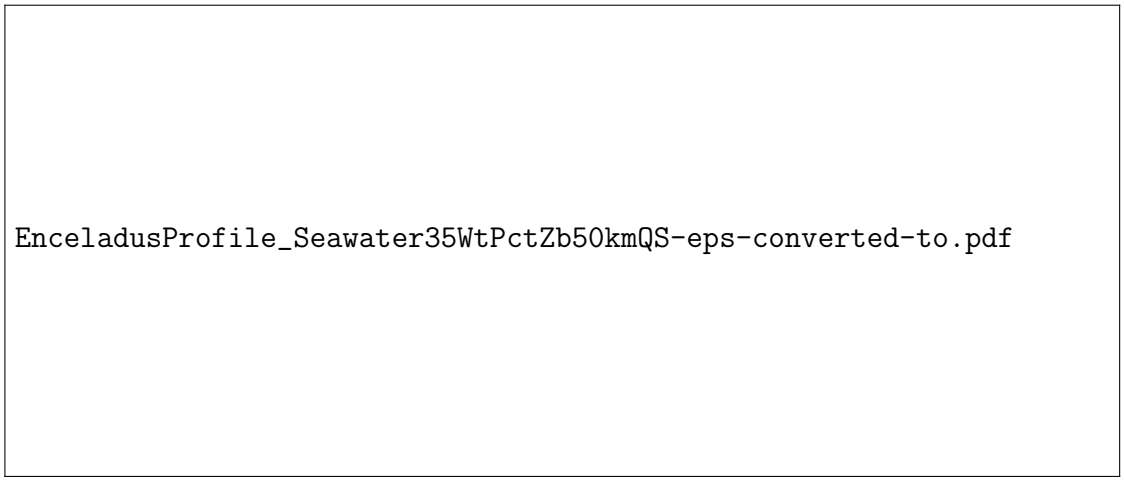

Figure S5. Enceladus: global interior structure with the ocean composition of seawater and ice Ih thickness of 50 km. Y-axis is radius (in km) for each of the three panels. Left: V_S (lines) and V_P (dashes). Middle: Pressure (lines), temperature (– –), and density (dot-dashes). Right: Anelasticity.

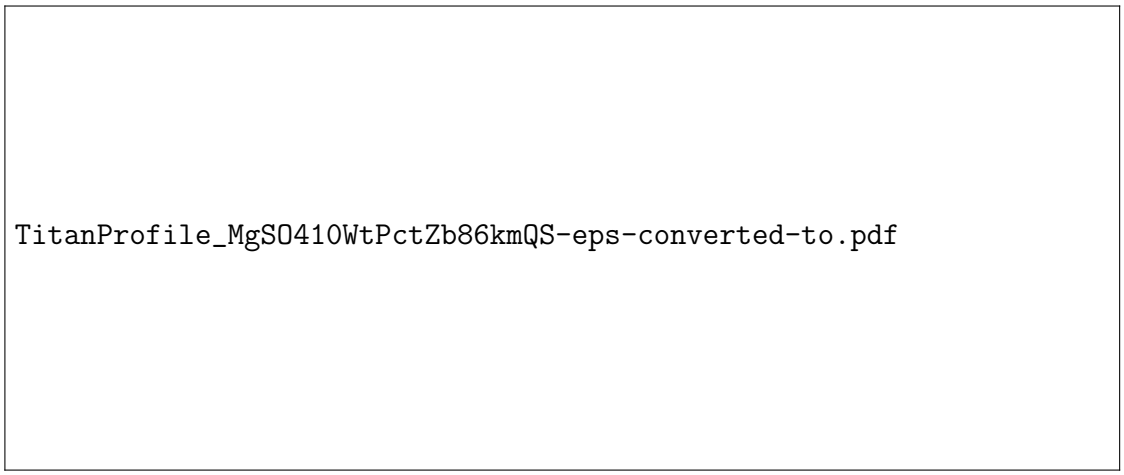

Figure S6. Callisto: global interior structure with 10 wt% $MgSO_4$(aq) and ice Ih thickness of 86 km. Left: V_S (lines) and V_P (dashes). Middle: Pressure (lines), temperature (dashes) and density (dot-dashes). Right: Anelasticity.

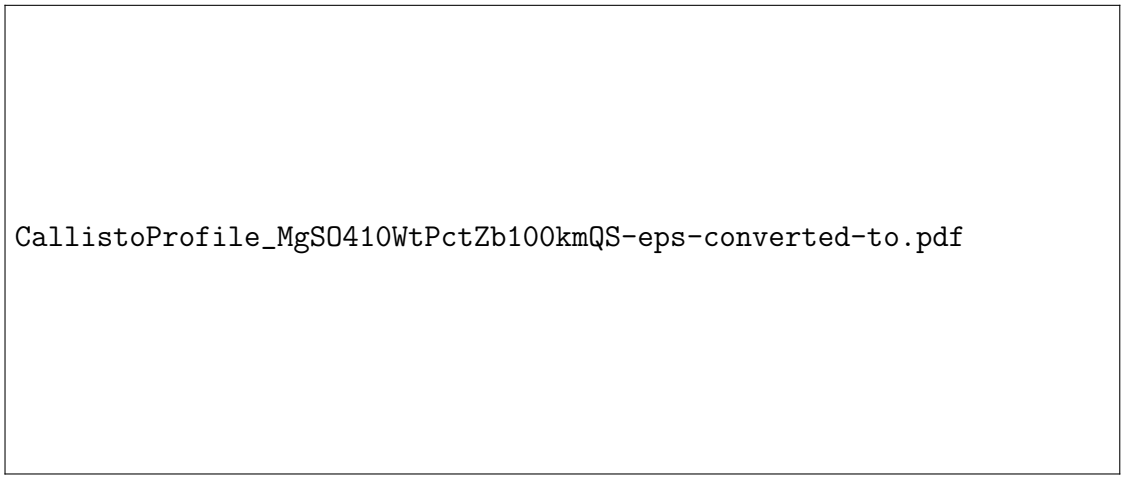

Figure S7. Callisto: global interior structure with 10 wt% $MgSO_4$(aq) and ice Ih thickness of 100 km. Left: V_S (lines) and V_P (dashes). Middle: Pressure (lines), temperature (dashes) and density (dot-dashes). Right: Anelasticity.